International Journal of Computational Methods
Vol. 13, No. 4 (2016) 1641003 (14 pages)

DOI: 10.1142/S0219876216410036



# ICCM2015(Paper ID:1148): DPD Simulation of the Movement and Deformation of Bioconcave Cells

L. W. Zhou
*Institute of Mechanics*
*Chinese Academy of Sciences*
*Beijing 100190, P. R. China*
*zhoulvwen@imech.ac.cn*

Yu-Qian Zhang
*Cancer Institute and Hospital*
*Chinese Academy of Medical Sciences*
*Beijing 100021, P. R. China*
*yqzhang.cams@gmail.com*

Xiao-Long Deng
*Beijing Computational Science Research Center*
*Beijing 100094, P. R. China*
*xiaolong.deng@csrc.ac.cn*

M. B. Liu*
*College of Engineering, Peking University*
*Beijing 100871, P. R. China*
*mbliu@pku.edu.cn*

Received 5 September 2015
Accepted 15 October 2015
Published 11 January 2016

This paper presents a dissipative particle dynamics (DPDs) method for investigating the movement and deformation of biconcave shape red blood cells (RBCs) with the worm-like chain (WLC) bead spring. First, the stretching of a RBC is modeled and the obtained shape evolution of the cell agrees well with experimental results. Second, the movement and deformation of a RBC in shear flows are investigated and three typical modes (tumbling, intermittent and tank-treading) are observed. Lastly, an illustrating example of multi-RBCs in Poiseuille flow in a tube is simulated. We conclude that the presented DPD method with WLC spring can effectively model the movement and deformation of bioconcave cells.

*Keywords*: Dissipative particle dynamics; cell model; cell movement; cell deformation.

*Corresponding author.

## 1. Introduction

The study of the movement and deformation of single cells in blood vessels is important for understanding mechanical properties of cells. The changes in mechanical properties of cells may be closely related to severe cell diseases. In cancer, the changes may be due to internal factors such as genetic mutation. For example, in malaria, the changes are probably due to external factors such as parasites and bioactive lipids [Hosseini *et al.* (2008)]. These changes are often promoted by the altering in the mechanical behaviors of living cells. Modern physiology and medicine have established the relationship of mechanical changes between healthy and pathological cells. For instance, diseased cells such as cancer cells are known to have different stiffness and elasticity compared to their healthy counterparts [Lee and Lim (2007)]. Such differences could be used to distinguish normal cells from diseased cells [Hou *et al.* (2009); Bathe *et al.* (2002)]. Recently, increased micro-fluidic devices were designed to diagnose and treat cells disease such as cancer as different cells can have different mechanical properties [Suresh (2007)]. It is therefore an important step to uderstand how cells move and deform respond to specific physical loads, and further infer mechanical properties of cells.

Continuum cell models are earlier and most commonly used approaches to model the mechanical dynamics of cells. Continuum models treat the cell as continuum material. Generally, continuum models can be classified into solid models and liquid drop models. The solid models usually assume the whole cell to be homogeneous without considering the distinct cortical layer. Practices show that solid models can usually achieve equilibrium with certain amount of load. For instance, even when the suction pressure greatly exceeds the critical suction pressure, endothelial cells and chondrocytes are unable to flow into the pipette [Jones *et al.* (1999)]. Another kind of continuum cell models is liquid drop models. By treating the cell as a liquid drop, liquid drop models can be used to model large cell deformations. The Newtonian liquid drop model was developed by Yeung and Evans [1989], and it can model large cell deformations well only when the progress is slow. In order to consider the effects of the nucleus on cell deformation, the compound drop model was developed, which assumed the nucleus to be an encapsulated liquid drop [Hochmuth *et al.* (1993)]. Compare with above-mentioned Newtonian liquid drop, the compound drop model can effectively explain the rapid initial response in micro-pipette aspiration and fast recoil on recovery [Tran-Son-Tay *et al.* (1998)]. Recently, Leong *et al.* [2011] presented a modified compound drop model, which can take account of stiffness, elasticity, and viscosity of both the cortex and the nucleus to model breast cancer cell entry into a constricted micro-channel. The modeled cell entry behavior agrees with experimental observations.

The continuum cell models are easy to implement and straightforward to use in computing the mechanical properties of the cells if the biomechanical response at the cell level is needed. However, they provide less insight into the detailed molecular mechanical events. For this reason, more accurate micro- and nanostructural models

were developed. The red blood cell (RBC) membrane is composed of a lipid bilayer and an attached cytoskeleton. The cytoskeleton consists primarily of spectrin proteins, which form the network by linking short actin filaments. Discher *et al.* [1998] and Li *et al.* [2005] developed the spectrin-level RBC model. The spectrin-level model corresponds to an effective spectrin network where each spring represents a single spectrin tetramer. The RBC is represented by a network of springs in combination with bending rigidity and constraints for surface-area and volume conservation. The spectrin-level RBC model was successfully validated against experimental data of the mechanical response of an individual cell. However, it involves limited degrees of freedom and application of the model in flow simulations requires prohibitively expensive computations. For this reason, Pivkin and Karniadakis [2008] developed a coarse-grained model based on the spectrin-level RBC model using mean-field theory and then applied it to dissipative particle dynamic (DPD) simulations in capillaries of $10\,\mu$m in diameter while the blood velocity is typically about 1 mm/s. The RBC was found to deform under certain flow conditions and, after some transition period, assumed the parachute-type shape, which is commonly observed in experiments [Tomaiuolo *et al.* (2007)]. A more rigorous and systematic procedure to derive coarse-grained RBC models was present by Fedosov *et al.* [2010]. The RBC is modeled by DPD particles and captures the elastic response at both small and large deformations. In addition, they also developed a stress-free model which avoids a number of pitfalls of existing RBC models, such as non-smooth or poorly controlled equilibrium shape and dependence of the mechanical properties on the initial triangulation quality. Fedosov *et al.* [2011] also extended this model to model adhesive dynamics of RBCs in Malaria.

In this work, the DPD are used to model movement and deformations of biconcave shape RBCs. Methodology of DPD and cell model are respectively described in Secs. 2 and 3. After then, the simulations and results of biconcave cells are presented and analyzed in Sec. 4, including RBC stretching, RBC in shear flow and multi-RBCs in Poiseuille flow in a tube. The paper concludes in Sec. 5 with some remarks.

## 2. Dissipative Particle Dynamics Methodology

In the present work, we construct cell model using DPD method. DPD is a relatively new mesoscale technique that can be used to simulate the behavior of fluids [Hoogerbrugge and Koelman (1992)]. In our DPD system, there are four types of particles, namely, wall particles, external fluid particles, membrane particles and internal fluid particles. The forces between particles are assumed to be pair-wise additive. The motion of DPD particles is governed by Newton's equations of motion. For a simple DPD particle $i$, we have the following governing equations:

$$\frac{\mathrm{d}\mathbf{r}_i}{\mathrm{d}t} = \mathbf{v}_i, \quad \frac{\mathrm{d}\mathbf{v}_i}{\mathrm{d}t} = \mathbf{f}_i^{\mathrm{ext}} + \sum_{j \neq i}^{N} \mathbf{f}_{ij}, \tag{1}$$

where $\mathbf{r}_i$ and $\mathbf{v}_i$ denote the position and velocity of particle $i$. The masses of DPD particles $m_i$ are usually taken to be the same as unity and $\mathbf{f}_{ij}$ denotes the total force between particles $i$ and $j$. $\mathbf{f}_i^{\text{ext}}$ is the external force, such as the gravity. The inter-particle force $\mathbf{f}_{ij}$ consists of three parts, namely conservative force $\mathbf{F}_{ij}^{\text{C}}$, dissipative force $\mathbf{F}_{ij}^{\text{D}}$ and random force $\mathbf{F}_{ij}^{\text{R}}$,

$$\mathbf{f}_{ij} = \mathbf{F}_{ij}^{\text{C}} + \mathbf{F}_{ij}^{\text{D}} + \mathbf{F}_{ij}^{\text{R}}. \tag{2}$$

The conservative force describes the thermodynamic behavior of the DPD system, and can be derived form a pair potential that acts between particles $i$ and $j$ as

$$\mathbf{F}_{ij}^{\text{C}} = \begin{cases} a_{ij}(1 - r_{ij}/r_c)\hat{\mathbf{r}}_{ij} & r_{ij} < r_c, \\ 0 & r_{ij} \geq r_c, \end{cases} \tag{3}$$

where $a_{ij}$ is the repulsion parameter between particles $i$ and $j$, and it represents the strength of the collision; $\mathbf{r}_{ij} = \mathbf{r}_i - \mathbf{r}_j$ represents the relative position between particle $i$ and particle $j$; $r_{ij} = |\mathbf{r}_{ij}|$, $\hat{\mathbf{r}}_{ij} = \mathbf{r}_{ij}/r_{ij}$ is the unit vector directed from the mass center of particle $j$ to $i$; and $r_c$ is the cut-off radius. Equation (3) indicates that the conservative force is repulsive over a limited radius $r_c$ only and acts in the direction of the $\hat{\mathbf{r}}_{ij}$ vector. The dissipative force describes the viscous effects of the DPD system and it acts like a viscous damper by reducing the relative velocity between DPD particles. The random force represents the thermal motion of unresolved scales, such as the molecules inside each particle. The dissipative force and random force are written as

$$\mathbf{F}_{ij}^{\text{D}} = -\gamma w^{\text{D}}(r_{ij})(\hat{\mathbf{r}}_{ij} \cdot \mathbf{v}_{ij})\hat{\mathbf{r}}_{ij}, \quad \mathbf{F}_{ij}^{\text{R}} = \sigma w^{\text{R}}(r_{ij})\xi_{ij}\hat{\mathbf{r}}_{ij}, \tag{4}$$

where $\gamma$ and $\sigma$ are two coefficients which represent the amplitude of the dissipative and random force. $w^{\text{D}}(r_{ij})$ and $w^{\text{R}}(r_{ij})$ are two weight functions which describe the variation of the friction coefficient and the noise amplitude with distance. $\mathbf{v}_{ij}(= \mathbf{v}_i - \mathbf{v}_j)$ represents the relative velocities between particle $i$ and particle $j$. $\xi_{ij}$ is a random variable with Gaussian statistics. For correct isothermal balance, the coefficients ($\gamma$ and $\sigma$) and the weight functions ($w^{\text{D}}$ and $w^{\text{R}}$) must satisfy two requirements [Espaol and Warren (1995)]

$$\gamma = \frac{\sigma^2}{2k_B T}, \quad w^{\text{D}}(r) = [w^{\text{R}}(r)]^2, \tag{5}$$

where $k_B$ is the Boltzmann constant and $T$ is the absolute temperature. There are different forms of $w^{\text{D}}(r)$ and $w^{\text{R}}(r)$, one simple, straightforward and commonly used choice is

$$w^{\text{D}}(r) = [w^{\text{R}}(r)]^2 = \begin{cases} (1 - r/r_d)^s & r < r_d, \\ 0 & r \geq r_d, \end{cases} \tag{6}$$

where $r_d$ is the cut-off distance for the dissipative and random forces and it may not be different from $r_c$, which is the cut-off distance for conservative force. The choice of $r_d$ affects the number of pairs of interacting particles and the computation

cost. The choice of $s$ can affects the strength of dissipative force between particles to influence viscosity and Schmidt number. In conventional DPD formulation, the choices are $s = 2$ and $r_c = r_d = 1$.

## 3. Cell Model

### 3.1. *Cell membrane model*

A biological cell may be regarded as a capsule enclosed by a semipermeable membrane and containing an internal fluid. The membrane of the cell may strongly conserve area and volume of the cell, and exhibits viscoelastic characteristics [Pozrikidis (2003)]. In this section, we employ the DPD particles and worm-like chain (WLC) spring model to construct the cell membrane. Figure 1 illustrates the sketch of cell membrane. The cell membrane is represented by a network of particles (beads) connected by WLC springs in DPD system, and surrounded by separate fluids. Similar to fluid particles that can be thought of as small regions of fluid; the membrane beads can be thought of as a patch of cell membrane consisting of number of monomeric units. The membrane beads exchange momentum with each other according to the spring force and DPD interactions. Hydrodynamic and thermodynamic interactions between the cell membrane and solvent then emerge naturally in these simulations.

Specifically, the cell membrane structure is defined by a two-dimensional triangular network on the surface. Each link of triangular network is modeled by nonlinear WLC spring model. The force between membrane particles includes the elastic and viscous parts. The elastic part is characterized by an energy potential, given by

$$\mathbf{f}_i^{\text{elastic}} = -\frac{\partial U(\{\mathbf{r}_i\})}{\partial \mathbf{r}_i}, \quad U(\{\mathbf{r}_i\}) = U_{\text{in-plane}} + U_{\text{bending}} + U_{\text{area}} + U_{\text{volume}}. \tag{7}$$

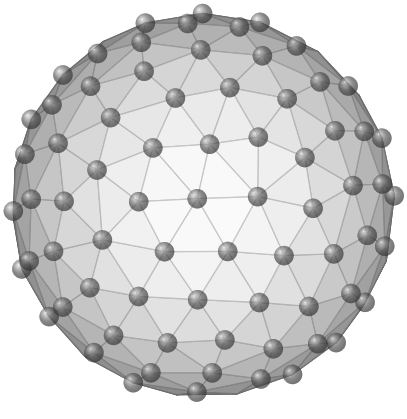

Fig. 1. Cell membrane represented by a network of springs linked DPD particles.

The in-plane energy term $U_{\text{in-plane}}$ indicates the elastic energy stored in the membrane, and it is assumed to have the form as follows [Marko and Siggia (1995)]

$$U_{\text{in-plane}} = \sum_{i \in 1 \cdots N_s} \left( \frac{k_B T l_i^{\max}}{4 p_i} \frac{3x_i^2 - 2x_i^3}{1 - x_i} + \frac{k_i}{x_i} \right), \tag{8}$$

where $N_s$ is the number of chains; $x_i = l_i / l_i^{\max} \in (0, 1)$, $l_i$ and $l_i^{\max}$ are the current and maximum length of spring $i$; $p_i$ is the persistence length; and $k_k$ is the power force coefficient. The first term in parentheses of Eq. (8) is derived from nonlinear WLC spring model. Taking into account dissipative forces of DPD, the first term in parentheses of Eq. (8) defines the contribution of viscoelastic springs. It should be note that WLC springs exert purely attractive forces, thus they produce a triangular area compression. While the second term in parentheses of Eq. (8), which provides triangular area expansion, contains a hydrostatic elastic energy of the triangular membrane patches. The minimum energy state of a single triangle corresponds to an equilibrium spring length $l_0$, which depends on the spring parameters and $k_i$. The relationship between the equilibrium length and these parameters can be determined by minimizing potential energy, or by setting the Cauchy stress obtained from the virial theorem to zero.

The bending energy term $U_{\text{bending}}$ in Eq. (7), represents the bending resistance of the lipid bilayer, and is assumed as follows [Fedosov *et al.* (2010)]:

$$U_{\text{bending}} = \sum_{i \in 1 \cdots N_s} k_b [1 - \cos(\theta_i - \theta_i^0)], \tag{9}$$

where $k_b$ is the bending constant; $\theta_i$ is the instantaneous angle between two adjacent triangles having a common edge, and $\theta_i^0$ is the spontaneous angle.

The area and volume restraint energy term $U_{\text{area}}$ and $U_{\text{volume}}$ are to constraint membrane surface area and cell volume conservation, respectively. The area and volume conservation restraint are given by [Fedosov *et al.* (2010)]:

$$U_{\text{area}} = \frac{k_a^{\text{global}} (A_{\text{tot}} - A_{\text{tot}}^0)^2}{2 A_{\text{tot}}^0} + \sum_{i \in 1 \cdots N_t} \frac{k_a^{\text{local}} (A_i - A_i^0)^2}{2 A_i^0}, \tag{10}$$

$$U_{\text{volume}} = \frac{k_v (V_{\text{tot}} - V_{\text{tot}}^0)^2}{2 V_{\text{tot}}^0}, \tag{11}$$

where $k_a^{\text{global}}$ and $k_a^{\text{local}}$ are the global and local area restraint constant; $A_{\text{tot}}$ and $A_{\text{tot}}^0$ are the current and desired areas of the cell membrane; $A_i$ and $A_i^0$ are the current and desired areas of the $i$th triangle; $k_v$ is the volume restraint constant; $V_{\text{tot}}$ and $V_{\text{tot}}^0$ are the current and desired global volume of the cell. The conservations of area and volume are achieved by increasing the global and local area restraint constant and volume restraint constant.

A biological cell membrane is known to be viscoelastic. Although the dissipative part in DPD model contributes to the membrane viscosity, its contribution is insufficient for a regular dissipative coefficient $\gamma_{ij}$. To incorporate viscous dissipation of

the lipid bilayer into the cell membrane properly, we follow the general framework of the fluid particle model [Fedosov *et al.* (2010); Espaol (1998)] to define an additional dissipative force $\mathbf{F}_{ij}^{\mathrm{D,vis}}$ for each spring as

$$\mathbf{F}_{ij}^{\mathrm{D,vis}} = -\gamma^{\mathrm{T}}\mathbf{v}_{ij} - \gamma^{\mathrm{C}}(\mathbf{v}_{ij}\cdot\hat{\mathbf{r}}_{ij})\hat{\mathbf{r}}_{ij}, \tag{12}$$

where $\gamma^{\mathrm{T}}$ and $\gamma^{\mathrm{C}}$ are dissipative parameters, $\mathbf{v}_{ij}$ is the relative velocity of two beads of one spring. To balance the temperature of the cell membrane via a fluctuation-dissipation theorem, an additional random force $\mathbf{F}_{ij}^{\mathrm{R,vis}}$ must added to each spring

$$\mathbf{F}_{ij}^{\mathrm{R,vis}} = \sqrt{2k_BT}(\sqrt{2\gamma^{\mathrm{T}}}d\overline{\mathbf{W}}_{ij}^{S} + \frac{1}{3}\sqrt{3\gamma^{\mathrm{C}}-\gamma^{\mathrm{T}}}\mathrm{tr}[d\mathbf{W}_{ij}]\mathbf{I})\hat{\mathbf{r}}_{ij}, \tag{13}$$

where $\mathbf{I}$ is the unit second-order tensor, $\mathrm{tr}[d\mathbf{W}_{ij}]$ is the trace of a random matrix of independent Wiener increments $d\mathbf{W}_{ij}$, and $d\overline{\mathbf{W}}_{ij}^{S} = \mathbf{W}_{ij}^{S} - \mathrm{tr}[d\mathbf{W}_{ij}^{S}]\mathbf{I}/3$ is the traceless symmetric part. The general fluid particle model not only provides the enough membrane viscosity but also ensures the momentum conservation.

### 3.2. *Parameters determination*

Before simulation, we must determinate several parameters in the membrane network model. In order to connect the above-described cell model to the macroscopic properties of cell, a relationship between macroscopic elastic properties (shear, area-compression and Young's moduli) of the network and model parameters has to be derived. Linear analysis [Dao *et al.* (2006)] for a regular hexagonal network on the cell membrane was applied to obtain its linear macroscopic properties with respect to the selected network parameters. The membrane shear modulus is given by [Fedosov *et al.* (2010)]

$$\mu_0 = \frac{\sqrt{3}k_BT}{4p_il_{i,0}}\left(\frac{x_0}{2(1-x_0)^3} - \frac{1}{4(1-x_0)^2} + \frac{1}{4}\right) + \frac{2\sqrt{3}k_p}{4l_{i,0}^3}, \quad x_0 = l_{j,0}/l_j^{\max}, \tag{14}$$

where the subscript "0" refers to the stress-free state. The corresponding linear-elastic area-compression moduli $K$ and Young's moduli $Y$ are given as

$$K = 2\mu_0 + k_a^{\mathrm{global}} + k_a^{\mathrm{local}}, \quad Y = \frac{4K\mu_0}{K+\mu_0}. \tag{15}$$

Equating the macroscopic bending energy of the Helfrich model [Helfrich (1973)] and the bending energy of the network model $U_{\mathrm{bending}}$, yields that the macroscopic bending rigidity $E_{\mathrm{B}}$ of the Helfrich model can be expressed in terms of the bending coefficient $k_b$ of Eq. (9) as [Fedosov *et al.* (2010)]

$$E_{\mathrm{B}} = \frac{2}{\sqrt{3}}k_b. \tag{16}$$

To simplify the general framework of the fluid particle model, $\gamma^{\mathrm{T}}$ was setted as $3\gamma^{\mathrm{C}}$ in Eqs. (12) and (13). The viscosity of cell membrane is therefore dependent on the dissipative part of DPD model and the additional viscous part

$$\mu_m = \sqrt{3}\gamma^{\mathrm{T}} + \frac{\sqrt{3}\gamma^{\mathrm{C}}}{4}. \tag{17}$$

### 3.3. *Scaling of model and physical units*

DPD simulations are conventionally performed in nondimensionalized or reduced units, based on the characteristic physical dimensions of the system. In present paper, the characteristic scale for length, energy unit and time [Fedosov *et al.* (2010)] is

$$\lambda = \frac{D^{\mathrm{P}}}{D^{\mathrm{M}}}, \quad \varepsilon = \frac{Y^{\mathrm{P}}}{Y^{\mathrm{M}}} \left(\frac{\lambda}{[\mathrm{m}]}\right)^2 (k_B T)^{\mathrm{P}}, \quad \tau = \left(\frac{D^{\mathrm{P}}}{D^{\mathrm{M}}} \frac{\eta^{\mathrm{P}}}{\eta^{\mathrm{M}}} \frac{Y^{\mathrm{M}}}{Y^{\mathrm{P}}}\right)^{\alpha}, \tag{18}$$

where the superscript "M" and "P" indicate "model" and "physics", respectively. $D$ denote the cell diameter, $Y$ denote Young's modulus and $\eta$ is viscosity.

## 4. Simulations and Results

In this section, single RBC is first studied by DPD simulations. Simulations include RBC stretching and RBC in shear flow. Then, the simulation of multi-RBCs in Poiseuille flow in a tube is presented.

### 4.1. *Stretching of a single RBC*

An RBC has a biconcave shape. All healthy mammalian RBCs unstressed shapes are disc-shaped (discocyte) [Diez-Silva *et al.* (2010)]. The biconcave discocyte RBC has a flexible membrane with a high surface-to-volume ratio that facilitates large reversible elastic deformation of the RBC as it repeatedly passes through small capillaries during microcirculation. RBC deformability is critical for circulation, which is necessary for RBCs squeezing through capillaries with smaller diameters than itself to deliver oxygen to various parts of the body. Pathological conditions affecting RBCs can lead to significant alterations to the discocyte shape due to the intracellular structural changes. The pathological RBCs are too stiff to deform sufficiently to traverse narrow capillaries. Instead they may disrupt the blood flow and block the capillaries, possibly leading to anemia and can even causing death.

Here, we perform RBC stretching simulations and compare the results with the experiment results. The unstressed RBC is assumed that its diameter $D_0 = 7.8\,\mu$m, the Young's modulus $Y_0 = 18.9\,\mu$N/m, the bending rigidity $E_B = 2.4 \times 10^{-19}$J and the viscosity of membrane $\eta_m = 0.02\,\mathrm{Pa}\cdot\mathrm{s}$. In DPD simulation, parameters of cell

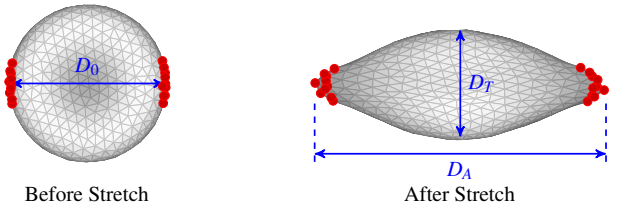


Fig. 2. Shapes of RBC before and after stretching.

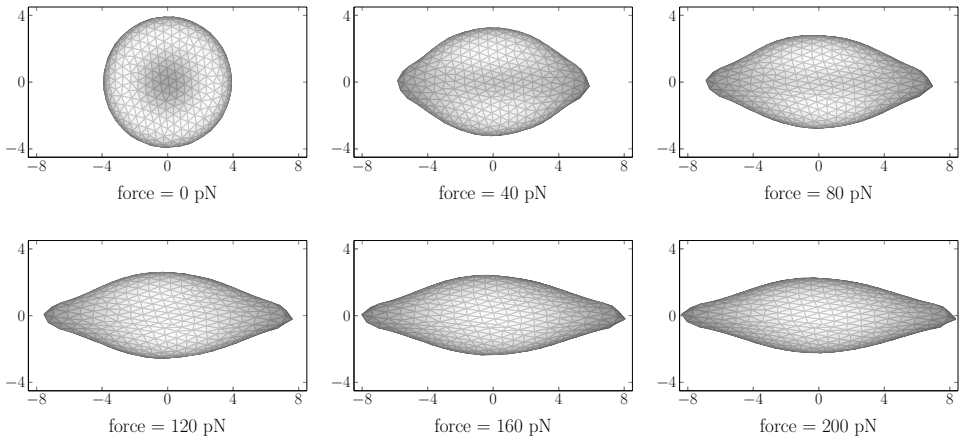


Fig. 3. RBC shape evolution at different stretch force.



model are taken as follows: $D_0^{\mathrm{M}} = 8.06$, $\mu_0^{\mathrm{M}} = 100$, $k_a^{\mathrm{global}} = 4{,}900$, $k_a^{\mathrm{local}} = 100$ and $k_v = 5{,}000$. Figure 2 shows the shapes of RBC before and after stretching. The total stretching force is in the range of $0 \sim 200$ pN, and is applied to the outermost 20% beads (drawn as small ball in Fig. 2).

Figure 3 shows final shapes after deformation under different stretching force. RBCs subjected to stretching are rotated in $y$–$z$ plane as observed in our simulations, and therefore measurements from a single observation angle may result in under-prediction of the maximum transverse diameter. With the increase of the stretching force, it is more and more difficult to elongate longer for RBC. There is no obvious difference between the RBC's final shapes at the stretching force of 160 pN and 200 pN, while the earliest stretching force of 40 pN caused significant deformation.

Figure 4 shows the stretching response of RBC at different stretching force. The experimental results [Suresh *et al.* (2005)] and the spectrin-level RBC models results [Dao *et al.* (2006)] are also included in Fig. 4. We find that we obtained similar results with those of Fedosov *et al.* [2010]. Our simulation results make an excellent agreement of the experimental results. The simulation results remain within the experimental error bars.

### 4.2. *Movement and deformation of a single RBC in shear flows*

Next, we perform RBC in shear flow simulations and compare the results with the experiment results. In our simulations, a RBC is suspended in a solvent and placed between two parallel walls moving with constant velocities in opposite direction. Experimental observations [Abkarian *et al.* (2007); Fischer (2004, 2007); Tran-Son-Tay *et al.* (1984)] of RBC dynamics in shear flow show RBC tumbling at low shear rates and tank-treading at high shear rates. Figure 5 shows snapshots of RBC in

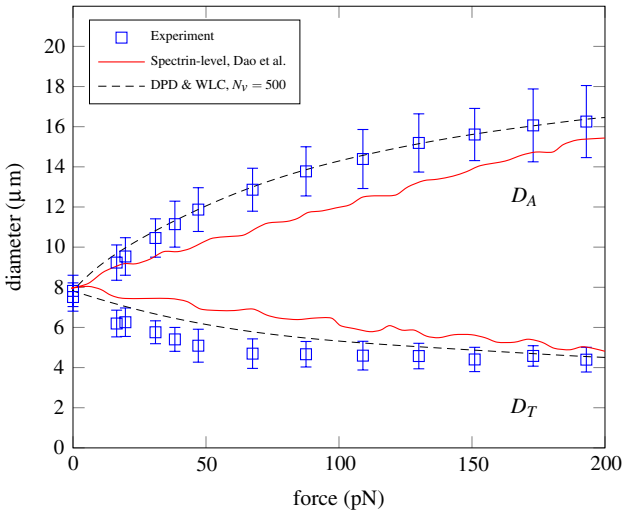


Fig. 4. Computational results of RBC stretching compared with the experiments and the specrin-level RBC model.

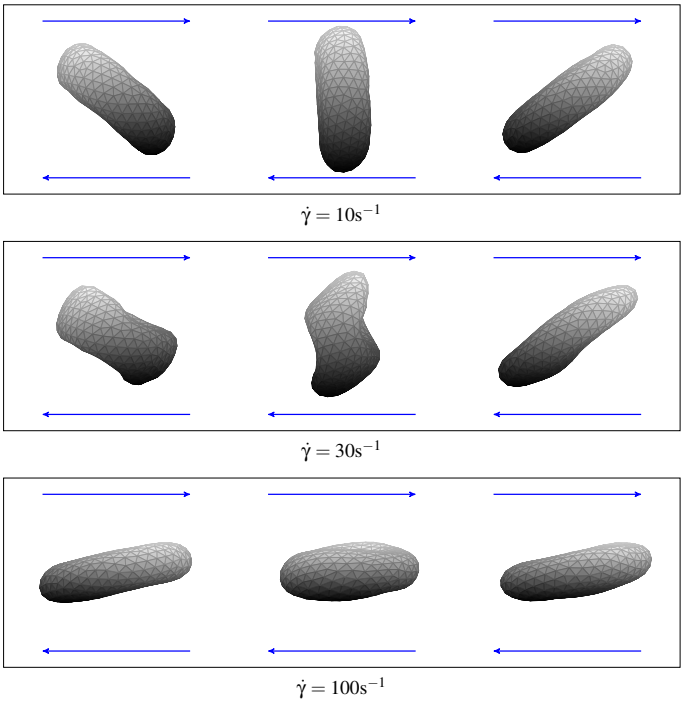


Fig. 5. Snapshots of RBC in different shear rate flow.

different shear rate flow from our simulations. Results of our simulations show RBC tumbling at shear rate $\dot{\gamma} = 10\,\mathrm{s}^{-1}$, tank-treading at shear rate $\dot{\gamma} = 100\,\mathrm{s}^{-1}$, and tumbling-to-tank-treading transition at shear rate $\dot{\gamma} = 30\,\mathrm{s}^{-1}$. The results show a negligible deformation during tumbling behavior, small shape deformations during tank-treading right after the transition, and significant shape deformations during tumbling-to-tank-treading transition.

Figure 6 shows RBC tumbling and tank-treading frequencies for different simulation setups versus shear rates in comparison with the experiments [Tran-Son-Tay *et al.* (1984)]. Computational results show a good agreement with the experimental results. From Fig. 6, we can see that according to the slope the profile of DPD simulation can be further divided into three distinct portions, namely tumbling region at low shear rate, intermittent region at medium shear rate and tank-treading at height shear rate. The profile of DPD is linear at each of three regions. It indicates that the frequencies of RBC increase linearly with the increase of shear rate. The intermittent region is very narrow and it is not convenient to observe in the experiment. Similar results for the intermittent region were reported in simulations of viscoelastic vesicles by Kessler *et al.* [2008].

### 4.3. *Movement and deformation of multiple RBCs in a tube*

Based on the properly simulations of a single RBC with accurate mechanics, rheology and dynamics, more complicated situations can further be simulated. One of those situations is blood flow. Figure 7 shows a DPD simulation of multi-RBCs in Poiseuille flow in a tube. The tube is modeling by two stationary parallel solid flat plates. The computational domain is 120 in length and has a square cross section

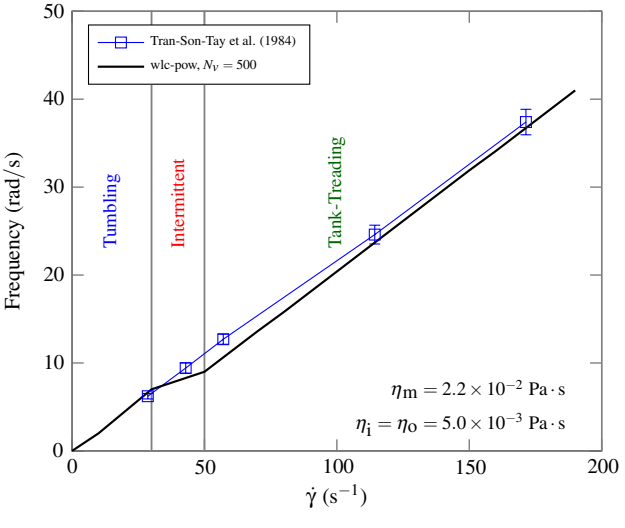


Fig. 6. Computational results of RBC in shear flow compared with the experiments.

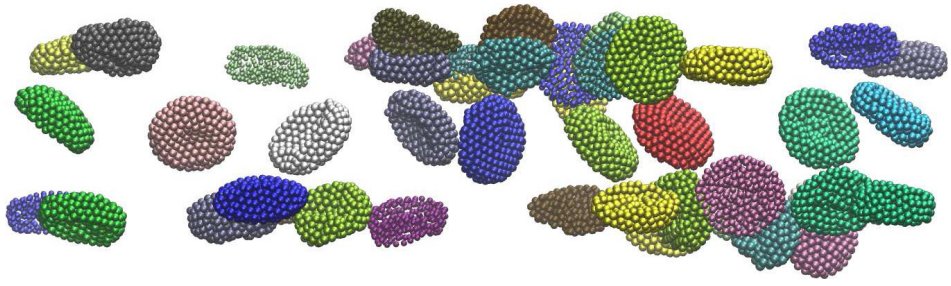

Fig. 7. A snapshot of multi-RBCs in Poiseuille flow in a tube. Fluid particles and wall particles have been omitted.



area of $15 \times 15$. A total number of 109192 DPD particles are used, including 71344 fluid particles and 60 RBCs placed in the planar slit and 21600 wall particles located in three layers parallel to the $x$–$y$ plane in each side. The periodic boundary conditions are applied to fluid boundaries in the $x$ and $y$ directions. On the surface of solid walls, we applied Maxwellian reflection boundary conditions to yield the no slip boundary condition [Revenga *et al.* (1999)]. The flow is driven by a uniform body force per unit mass applied to both fluid and RBC particles in the $x$ direction.

As an initial condition, RBCs were placed regularly within the tube. After the flow was turned on, the simulations were achieve steady state by enough time. Then, many properties of blood flow can be quantitatively calculated.

## 5. Conclusion

In this work, we use DPD method and WLC bead spring to model the movement and deformation of bioconcave cells and the DPD model can describe Young's modulus, bending rigidity, and viscosity of the cell membrane. The cell membrane is represented by a network of DPD particles connected by WLC springs.

Single biconcave discocyte RBC is simulated, including RBC stretching, RBC in shear flows. For RBC stretching, Cells' final shape and maximum transverse diameter are measured quantitatively. For RBC in shear flows, tumbling and tank-treading frequencies are obtained from simulations. The simulation results of both RBC stretching and RBC in shear flows agree with experimental observations. After then, multi-RBCs in Poiseuille flow in a tube are also simulated. From the testing examples, it can be concluded that the presented DPD method with WLC spring can effectively model the movement and deformation of single RBC and multi-RBCs in different flow situations.

## Acknowledgments

This work was partially supported by the National Natural Science Foundation of China (Grant Nos. 31370953, 10942004 and 91230203).

## References

Abkarian, M., Faivre, M. and Viallat, A. [2007] "Swinging of red blood cells under shear flow," *Phys. Rev. Lett.* **98**, 188302.

Bathe, M., Shirai, A., Doerschuk, C. M. and Kamm, R. D. [2002] "Neutrophil transit times through pulmonary capillaries: The effects of capillary geometry and fMLP-stimulation," *Biophys. J.* **83**(4), 1917–1933.

Dao, M., Li, J. and Suresh, S. [2006] "Molecularly based analysis of deformation of spectrin network and human erythrocyte," *Mater. Sci. Eng. C.* **26**, 1232–1244.

Discher, D. E., Boal, D. H. and Boey, S. K. [1998] "Simulations of the erythrocyte cytoskeleton at large deformation. II. Micropipette aspiration," *Biophys. J.* **75**(3), 1584–1597.

Diez-Silva, M., Dao, M., Han, J., Lim, C.-T. and Suresh, S. [2010] "Shape and biomechanical characteristics of human red blood cells in health and disease," *MRS Bull. Mater. Res. Soc.* **35**, 382–388.

Espaol, P. [1998] "Fluid particle model," *Phys. Rev. E.* **57**, 2930–2948.

Espaol, P. and Warren, P. [1995] "Statistical mechanics of dissipative particle dynamics," *Europhys. Lett.* **30**(4), 191–196.

Fedosov, D. A., Caswell, B. and Karniadakis, G. E. [2010] "Systematic coarse-graining of spectrin-level red blood cell models," *Comput. Meth. Appl. Mech. Eng.* **199**(29), 1937–1948.

Fedosov, D. A., Caswell, B. and Karniadakis, G. E. [2011] "Wall shear stress-based model for adhesive dynamics of red blood cells in malaria," *Biophys. J.* **100**(9), 2084–2093.

Fischer, T. M. [2004] "Shape memory of human red blood cells," *Biophys. J.* **86**, 3304–3313.

Fischer, T. M. [2007] "Tank-tread frequency of the red cell membrane: Dependence on the viscosity of the suspending medium," *Biophys. J.* **93**, 2553–2561.

Helfrich, W. [1973] "Elastic properties of lipid bilayers: Theory and possible experiments," *Z. Fr Naturforschung Teil C Biochem. Biophys. Biol. Virol.* **28**, 693–703.

Hochmuth, R., Ting-Beall, H., Beaty, B., Needham, D. and Tran-Son-Tay, R. [1993] "Viscosity of passive human neutrophils undergoing small deformations," *Biophys. J.* **64**(5), 1596–1601.

Hosseini, S. Majid and Feng, James J. [2008] "A particle-based model for the transport of erythrocytes in capillaries," *Chem. Eng. Sci.* **64**, 4488–4497.

Hoogerbrugge, P. J. and Koelman, J. [1992] "Simulating microscopic hydrodynamic phenomena with dissipative particle dynamics," *Europhys. Lett.* **19**, 155–160.

Hou, H., Li, Q., Lee, G., Kumar, A., Ong, C. and Lim, C. [2009] "Deformability study of breast cancer cells using microfluidics," *Biomed. Microdev.* **11**(3), 557–564.

Jones, W. R., Ping Ting-Beall, H., Lee, G. M., Kelley, S. S., Hochmuth, R. M. and Guilak, F. [1999] "Alterations in the Young's modulus and volumetric properties of chondrocytes isolated from normal and osteoarthritic human cartilage," *J. Biomech.* **32**(2), 119–127.

Kessler, S., Finken, R. and Seifert, U. [2008] "Swinging and tumbling of elastic capsules in shear flow," *J. Fluid Mech.* **605**, 207–226.

Lee, G. Y. and Lim, C. T. [2007] "Biomechanics approaches to studying human diseases," *Trends Biotechnol.* **25**(3), 111–118.

Leong, F. Y., Li, Q., Lim, C. T. and Chiam, K.-H. [2011] "Modeling cell entry into a micro-channel," *Biomech. Model. Mechanobiol.* **10**(5) 755–766.

Li, J., Dao, M., Lim, C. and Suresh, S. [2005] "Spectrin-level modeling of the cytoskeleton and optical tweezers stretching of the erythrocyte," *Biophys. J.* **88**(5), 3707–3719.

Marko, J. F. and Siggia, E. D. [1995] "Stretching DNA," *Macromolecules* **28**, 8759–8770.

Pivkin, Igor, V. and Karniadakis, George, E. M. [2008] "Accurate coarse-grained modeling of red blood cells," *Phys. Rev. Lett.* **101**, 118105.

Pozrikidis, C. [2003] *Modeling and Simulation of Capsules and Biological Cells*, 1st edn. (Chapman and Hall/CRC, Boca Raton, FL).

Revenga, M., Zuniga, I. and Espanol, P. [1999] "Boundary conditions in dissipative particle dynamics," *Comput. Phys. Commun.* **121**(1), 309–311.

Suresh, S. [2007] "Biomechanics and biophysics of cancer cells," *Acta Materialia* **55**(12), 3989–4014.

Suresh, S., Spatz, J., Mills, J. P., Micoulet, A., Dao, M., Lim, C. T., Beil, M. and Seufferlein, T. [2005] "Connections between single-cell biomechanics and human disease states: Gastrointestinal cancer and malaria," *Acta Biomater* **1**, 15–30.

Tomaiuolo, G., Preziosi, V., Simeone, M., Guido, S., Ciancia, R., Martineelli, V., Rinaldi, C. and Rotoli, B. [2007] "A methodology to study the deformability of red blood cells flowing in microcapillaries *in vitro*," *Annali dell'Istituto superiore di sanit* **43**(2), 186–192.

Tran-Son-Tay, R., Sutera, S. P. and Rao, P. R. [1984] "Determination of red blood cell membrane viscosity from rheoscopic observations of tank-treading motion," *Biophys. J.* **46**, 65–72.

Tran-Son-Tay, R., Kan, H.-C., Udaykumar, H., Damay, E. and Shyy, W. [1998] "Rheological modeling of leukocytes," *Med. Biol. Eng. Comput.* **36**(2), 246–250.

Yeung, A. and Evans, E. [1989] "Cortical shell-liquid core model for passive flow of liquid-like spherical cells into micropipets," *Biophys. J.* **56**(1), 139–149.